Remote Sensing of Environment 114 (2010) 1924–1939

Contents lists available at ScienceDirect

Remote Sensing of Environment

journal homepage: www.elsevier.com/locate/rse

Evaluating evapotranspiration and water-use efficiency of terrestrial ecosystems in the conterminous United States using MODIS and AmeriFlux data

Xiaoliang Lu *, Qianlai Zhuang

Departments of Earth & Atmospheric Sciences and Agronomy, Purdue University, West Lafayette, IN, 47907, United States

ARTICLE INFO

Article history:
Received 29 July 2009
Received in revised form 2 April 2010
Accepted 3 April 2010

Keywords:
MODIS
Evapotranspiration
Artificial neural networks
Water-use efficiency

ABSTRACT

In this study, we used the remotely-sensed data from the Moderate Resolution Imaging Spectrometer (MODIS), meteorological and eddy flux data and an artificial neural networks (ANNs) technique to develop a daily evapotranspiration (ET) product for the period of 2004–2005 for the conterminous U.S. We then estimated and analyzed the regional water-use efficiency (WUE) based on the developed ET and MODIS gross primary production (GPP) for the region. We first trained the ANNs to predict evapotranspiration fraction (EF) based on the data at 28 AmeriFlux sites between 2003 and 2005. Five remotely-sensed variables including land surface temperature (LST), normalized difference vegetation index (NDVI), normalized difference water index (NDWI), leaf area index (LAI) and photosynthetically active radiation (PAR) and ground-measured air temperature and wind velocity were used. The daily ET was calculated by multiplying net radiation flux derived from remote sensing products with EF. We then evaluated the model performance by comparing modeled ET with the data at 24 AmeriFlux sites in 2006. We found that the ANNs predicted daily ET well ($R^2 = 0.52$–0.86). The ANNs were applied to predict the spatial and temporal distributions of daily ET for the conterminous U.S. in 2004 and 2005. The ecosystem WUE for the conterminous U.S. from 2004 to 2005 was calculated using MODIS GPP products (MOD17) and the estimated ET. We found that all ecosystems' WUE-drought relationships showed a two-stage pattern. Specifically, WUE increased when the intensity of drought was moderate; WUE tended to decrease under severe drought. These findings are consistent with the observations that WUE does not monotonously increase in response to water stress. Our study suggests a new water-use efficiency mechanism should be considered in ecosystem modeling. In addition, this study provides a high spatial and temporal resolution ET dataset, an important product for climate change and hydrological cycling studies for the MODIS era.

1. Introduction

The linkage between carbon (C) uptake and water cycling has been widely recognized (Running and Coughlan, 1988; Baldocchi and Harley, 1995; Baldocchi and Wilson, 2001). It is also recognized that plants tradeoff between water loss and C gain in photosynthesis through regulation of stomatal conductance (e.g., Collatz et al., 1991; Whitehead, 1998; Tenhunen et al., 1990). Therefore, water-use efficiency (WUE), defined in this study as the ratio between gross primary productivity (GPP) and evapotranspiration (ET), is an important index to study the survival, productivity and fitness of plants (Osmond et al., 1982). Moreover, the information on spatiotemporal patterns of ecosystem WUE can be useful to analyzing plant species distribution (Holdridge, 1947; Woodward, 1987; Hogg, 1994) and ecosystem carbon cycling (Schapendonk et al., 1997; Centritto et al., 2002). Traditionally, it is believed that WUE will be increased under water stress and drought condition due to a reduction in stomatal conductance. Moreover, this regulation of stomatal behavior is widely adopted in ecosystem models (Running and Hunt, 1993; Hunt et al., 1996). However, several studies showed that this mechanism might not hold especially under severe drought conditions (Reichstein et al., 2002, 2003; Medrano et al., 2009). Thus, a better knowledge of variability of WUE under drought condition is of importance to agricultural sector and climate change study of water, carbon, and energy cycling. To date, variations in WUE have been extensively studied at the individual leaf scale (Collatz et al., 1991; Jarvis, 1995; Medrano et al., 2009). However, most of them were focused on the changes under normal precipitation or moderate drought condition (Rammbal et al., 2003; Baldocchi, 1997; Williams et al., 1998), less focused on severe drought condition (e.g., Reichstein et al., 2002, 2007).

This study has two objectives: (1) to estimate ET for the conterminous U.S. (2) to analyze WUE responses to different level drought. We first quantified ET at a daily time step and a 4 km × 4 km spatial resolution for the conterminous U.S. by using artificial neural networks (ANNs). We then used MODIS gross primary production

* Corresponding author.
E-mail address: lxiaolia@purdue.edu (X. Lu).

0034-4257/$ – see front matter © 2010 Elsevier Inc. All rights reserved.
doi:10.1016/j.rse.2010.04.001

(GPP) and ET to calculate WUE. Specifically, we trained ANNs using AmeriFlux data and site-specific MODIS explanatory variables (AmeriFlux; Baldocchi et al., 2001). The ANNs performance on the site level was then verified using eddy flux data. The WUE response to drought was analyzed on the selected regions where there are large contrasts in terms of drought condition.

In Section 2, we summarize the methods of ET estimation based on remote sensing data. Section 3 describes the ANN method and required data, including a description of the AmeriFlux observations and the selection of explanatory variables. Section 4 verifies the ANNs at eddy flux tower sites. Section 5 describes the way to determine daily ET and WUE at a 4-km resolution for the conterminous U.S. from 2004 to 2005. Spatiotemporal patterns of and the relationship between WUE and drought are then analyzed.

2. Summary of satellite-based ET estimation

Although Kustas and Norman (1996) pointed out that remote sensing is the only method for efficiently estimating ET at a regional or continental scale, remotely-sensed ET estimation is far from satisfactory. ET is a complex process that is related to many variables, which cannot be detected directly by remote sensing techniques. However, ET can be indirectly estimated using remote sensing data by: (1) calculating ET as a residual of surface energy balance, where other energy components are estimated from satellites' measurements. The idea has been implemented in the Surface Energy Balance Algorithm for Land (SEBAL; Bastiaanssen et al., 1998a,b), the Surface Energy Balance System (SEBS; Su, 2002), and the resistance surface energy balance (RSEB; Kalma and Jupp, 1990); (2) applying physical models, such as the Penman–Monteith equation (Penman, 1948; Monteith, 1964; Zhang et al, 2008; Leuning et al, 2008), which use remote sensing data as forcing inputs or (3) using empirical methods that relate observable variables of satellites to ET.

For the first method, the estimate is based on the surface net radiation, which could be partitioned into three parts:

$$R_n = G + H + \lambda E \tag{1}$$

$$H = \rho^* C_\rho^* \frac{T_s - T_a}{R_a} \tag{2}$$

where H (W/m^2), and λE (W/m^2) are the fluxes of sensible heat, latent heat, respectively, R_n (W/m^2) is net radiation, G (W/m^2) is soil heat flux; T_s (K), T_a (K) are the aerodynamic surface and air temperature; R_a the aerodynamic resistance (s m^{-1}), determine the transfer of heat and water vapor from the evaporating surface into the air above the canopy, λ (J/kg) is the latent heat of vaporization, ρ (kg/m^3) is air density, and C_ρ (J/kg/K) is the specific heat capacity of air.

From Eq. (1), latent heat flux (ET) is thus the residual by subtracting soil heat and sensible heat fluxes from net radiation R_n. Many studies have provided methods to calculate H and G (Gao et al., 2008; Cleugh and Dunin, 1995; Hall et al., 1992; Kalma and Jupp, 1990). Although this residual approach is theoretically sound, its performance in practical applications suffered from strong assumptions needed to estimate H and G, which were well discussed by Cleugh et al. (2007).

Using the Penman–Monteith (Penman, 1948; Monteith, 1964) (hereafter P–M) theory is the second method to estimate ET (e.g., Zhuang et al., 2003

$$\lambda E = \frac{sA + \left(\rho^* C_\rho^* D_a / R_a\right)}{s + r(1 + R_s / R_a)} \tag{3}$$

where s is the slope of the curve relating saturation water vapor pressure to temperature; A is available energy ($R_n - G$) which is the sum of latent heat and sensible heat; D_a is the water vapor pressure deficit of the air; and R_a, R_s are the aerodynamic resistance and surface resistance (s m^{-1}), respectively. R_s describes the resistance of vapor flow through stomata openings and soil surface. The biggest challenge with the P–M method is to estimate the surface resistance when the method is applied on a large scale. Specially, the approximation processes in estimating R_a R_s and D_a reduce its theoretical integrity.

The third method is to use empirical approach to correlate remotely-sensed surface variables to ET. Much evidence shows that a scatter plot of remotely sensed surface temperature and normalized difference vegetation index (NDVI) is bounded by a triangle (Carlson et al., 1994, 1995a,b; Gillies and Carlson, 1995; Gilloes et al., 1997). Water availability is assumed not to be the limiting factor on the cold edge of the triangle; thus the potential ET is equal to actual ET. The actual ET is almost zero along the warm edge. This approach may be applicable for operational estimation of regional ET. The assumption that the effect of wind speed and humidity on the surface evaporation can be reflected in the derived radiometric surface temperature may hamper its precision on very large scales (Jiang and Islam, 2001). Fisher et al (2008) translated Priestley–Taylor estimates of potential evapotranspiration into rates of actual evapotranspiration by introducing remotely-sensed parameters.

Here, we combined some of the advantages of these techniques with an artificial neural networks (ANNs) learning approach and eddy flux and satellite data to develop an ET product for the conterminous U.S. Nonlinear relationships between chosen explanatory variables and ET were first trained using the AmeriFlux data. ET for the conterminous U.S. was then derived from the networks driven by remotely-sensed and meteorological data for developing and analyzing WUE for the conterminous U.S.

3. Method and data

3.1. Method

3.1.1. Neural networks for calculating evapotranspiration fraction (EF)

ET varies diurnally. It is a challenge to estimate ET using satellite observations, which are instantaneous measures. Here we calculated ET based on EF that is an almost constant during daytime hours (Shuttleworth et al., 1989; Sugita and Brutsaert, 1991; Crago, 1996; Crago and Brutsaert, 1996). EF, the ratio of latent heat to available energy, depends on land cover types (Crago and Brutsaert, 1996 Specifically, the EF was calculated as:

$$EF = \frac{ET}{A} \tag{4}$$

We assumed that instantaneous EF is nearly constant during a day. The daily ET was then calculated from daily net radiation and instantaneous EF as:

$$ET = \frac{86400^* EF^* R_n}{\lambda} \tag{5}$$

where λ is the latent heat of vaporization (J kg^{-1}).

The neural network technique is widely used for nonlinear functions approximation. In this study, the multilayer networks using the error back propagation algorithm (MLP-BP) (Haykin, 1998) were used to train the ANNs for EF. The first step in MLP-BP is to calculate the difference between the predicted and measured EF by propagating selected explanatory variables from network input to output. The errors are then propagated backward through the network to adjust weights in networks. These forward and backward propagations can be iterated till the residual error threshold (average squared error $<1\times10^{-5}$) is achieved. Normally, back-propagation uses a steepest descent method on error surfaces to adjust the weights to minimize the difference between the predicted and expected output, while it has the risk of being trapped in a local minimum. To

avoid the local optimal problem, a momentum term (Rumelhart et al., 1986) to the weight change was added in obtaining ANNs of EF.

3.1.2. Explanatory variable selection

At a leaf level, ET or evapotranspiration is affected by stomatal conductance, which is regulated by radiation intensity, vapor pressure deficit (VPD), soil water content and CO_2 concentrations, while regional ET is mainly affected by canopy structure, vegetation abundance and phenology, soil moisture, and energy on the top of the canopy and land surface.

The required VPD data were estimated based on satellite land surface temperature (LST) (Granger, 2000):

$$VPD = 0.668e^*(LST) - 0.015^*T_{\mathrm{ltm}} - 0.278 \quad (6)$$

where e^* (LST) is daily saturation vapor pressure, LST is radiative surface temperature from satellite data and T_{ltm} is long-term mean air temperature.

The normalized difference water index (NDWI) (Gao, 1996; Ceccato et al., 2001), which is based upon water absorption at 1240 nm, was used to measure vegetation liquid water content. Here we used the method developed by Gao (1996) to obtain the NDWI based on remotely sensed reflectance:

$$NDWI = \frac{p_{\mathrm{nir}} - p_{\mathrm{swir}}}{p_{\mathrm{nire}} + p_{\mathrm{swir}}} \quad (7)$$

where P_{swir}, P_{nir} are the reflectance at the short wave infrared (swir) and near infrared (nir) band. The NDWI is strongly correlated with leaf water content (Jackson et al., 2004) and soil moisture (Fensholt and Sandholt, 2003) over time. "Green" vegetation abundance information can be directly acquired from remote sensing by NDVI (Huete et al., 1994):

$$NDVI = \frac{p_{\mathrm{nir}} - p_{\mathrm{red}}}{p_{\mathrm{nire}} + p_{\mathrm{red}}} \quad (8)$$

where P_{red} is the reflectance at the red spectral band. Leaf area index is used to indicate phenology (Kang et al., 2003) and calculate evaporation of the intercepted liquid water. Incident photosynthetically active radiation (PAR)defined as illuminated solar radiation at the Earth's surface between 400 and 700 nm is used by plants in photosynthesis (Myneni et al., 2002). Previous studies showed that canopy photosynthesis increases with PAR (Baldocchi et al., 2003) and transpiration is thus expected to also increase with PAR.

When water vaporizing, the air above the evaporating surface becomes gradually saturated with water vapor. If this air is not continuously replaced with drier air, ET rate will decrease. Water vapor removal is mainly determined by wind speed and air turbulence as well as LST.

As explained above, we therefore selected LST, NDWI, NDVI, LAI, PAR, air temperature, wind velocity, and land cover types as explanatory variables for estimating EF with the ANN approach.

3.2. Data

To drive the neural network models at site-level and regional levels, we acquired four types of data: (1) tower-measured EF and explanatory datasets from AmeriFlux sites for ANNs' training and testing; (2) spatially-explicit explanatory datasets for the conterminous U.S., (3) datasets for calculating ET based on EF; and (4) MOD17 GPP data for WUE estimation. To apply the ANNs to the conterminous U.S., all input data were resampled and/or reprojected into the sinusoidal (SIN) projection at a 4-km resolution.

3.2.1. AmeriFlux data

We obtained the half-hourly EF based on the level 4 latent and sensible heat data at 28 AmeriFlux sites for the period 2003–2005 from (http://public.ornl.gov/ameriflux) (Fig.1; Table 1). These sites are distributed across the conterminous U.S, and cover a wide range of vegetation types (Baldocchi et al., 2001, Baldocchi, 2003). The level 4 product provides half-hourly air temperature, wind velocity and PAR measurements. To validate the performance of the ANNs, daily ET in 2006 on these towers were also collected. High-quality data were selected based on the quality assurance (QA) flags data.

All other explanatory variables including NDVI, LST, NDWI, LAI, and land cover were derived from MODIS data (Justice et al., 2002). MODIS provides data in 36 spectral bands and with the spatial resolution of 250 m, 500 m, and 1 km. Because NDVI and NDWI can be acquired from surface reflectance, we used the following four MODIS data products (Collection 5): (1) daily 1 km land surface reflectance (MOD09A1, Vermote and Vermeulen, 1999); (2) daily 1 km land surface temperature (MOD/MYD11A1, Wan et al., 2002); (3) 8-day, 1 km Leaf Area Index (LAI) (MOD15A2, Myneni et al., 2002); and (4) 1 km land cover (MOD12Q1, Friedl et al., 2002). Since LAI product is composited on an 8-day basis, we therefore assigned each 8-day composite LAI to the corresponding eight-day periods.

At a daily time step, we extracted 7×7 km regions from MODIS 1-km data centered on the flux towers. We averaged the values of each variable using the pixels with good quality within the area to represent the values at the flux site. If none of the values within the 7 km $\times$ 7 km area was of good quality, the period was assumed having no data. We categorized each site according to the University of Maryland land-cover classification system (UMD) (Friedl et al., 2002). To be consistent with the satellites overpass time (1030 and 1330 local time respectively), the half-hourly variables from the AmeriFlux sites in that time were selected to train the ANNs.

3.2.2. Regional data

To apply the ANNs to the conterminous U.S., we obtained MOD09A1, MOD/MYD11A1, MOD15A2 and MOD12Q1 in 2004 and 2005 from the Earth Observing System (EOS) Data Gateway (http://edcimswww.cr.usgs.gov/pub/imswelcome/). A total of 14 tiles were obtained to cover the whole study region. Daily NDWI and NDVI data were developed by using Eq. (8) and Eq. (9). For NDVI, NDWI and LAI, we replaced the poor quality data with the data generated using a moving average approach. We obtained the land cover type for each 4 km $\times$ 4 km cell by resampling the 1 km MODIS land cover map with the UMD classification system.

Because PAR is not a standard MODIS product, we used PAR datasets generated by Liang et al (2006) based on MODIS data in this study. After decoupling the correlation between surface reflectance and atmospheric properties, the authors used the look-up table made by Modtran (Berk et al., 1998) to calculate instantaneous PAR from top-of-atmosphere (TOA) radiance. Daily PAR was provided at a spatial resolution of 4 km. Daily mean PAR was estimated from two instantaneous PAR fluxes with the regression functions (Liang et al., 2006). We only obtained 3-year daily forcing data of PAR. Data in 2004 and 2005 were used for estimating ET and data in 2006 were used to validate site-level model performance.

From Terra and Aqua, we obtained two instantaneous LST measures. We calculated the daily daytime LST during daytime hours from the two values with an assumption that the diurnal surface temperature cycle can be approximated by the sinusoid function.

The daily meteorological inputs for the ANNs are air temperature and wind velocity. They were acquired from North American Regional Reanalysis (NARR, www.cdc.noaa.gov) datasets which are originally provided at a spatial resolution of 32 km under the Northern Lambert Conformal Conic coordinate system. The datasets cover the whole North American and have three time-steps: 3-hours, daily and monthly. We directly used the daily wind velocity dataset. Since ET almost only happens in daylight hours, we obtained daily air temperature during daytime hours by averaging 3-hours measurements. Both of them were resampled into a 4 km $\times$ 4 km resolution.

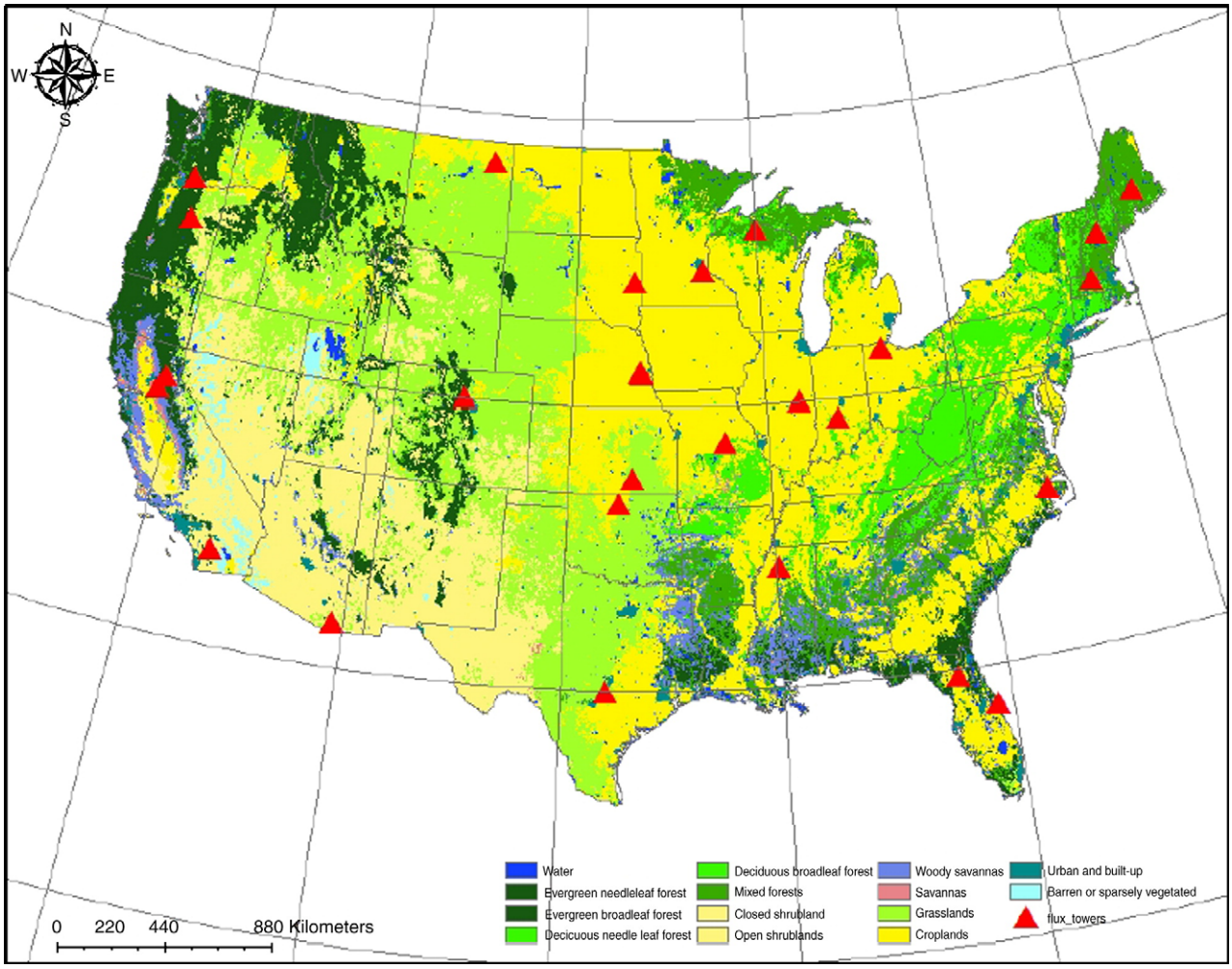

Fig. 1. Location and spatial distribution of the AmeriFlux sites used in this study. The base map is the MODIS UMD land-cover, which is used to drive regional ET quantification. Triangles indicate the location of the AmeriFlux sites.

3.2.3. Datasets for converting EF into ET

According to Eq. (4) and Eq. (5), net radiation and ground heat fluxes are needed to convert EF into ET. By checking soil heat flux fraction at most of sites, we assumed ground heat flux (G) is 15% of net radiation flux. The net radiation flux was estimated:

$$R_n = (1-a)^*S_{\text{in}} + (L_{\text{in}}-L_{\text{out}})-(1-\varepsilon_s)^*L_{\text{in}} \quad (9)$$

where a is surface albedo; S_{in} is the NARR estimate of shortwave radiation flux (W/m^2); L_{in} and L_{out} are the downward and upward long wave radiation flux (W/m^2), respectively and ε_s is the surface emissivity. L_{in} and L_{out} were estimated by:

$$L_{\text{in}} = \varepsilon_a \sigma T_a^4 \quad (10)$$

$$L_{\text{out}} = \varepsilon_s \sigma T_s^4 \quad (11)$$

where ε_a is the atmospheric emissivity; σ is the Stefan–Boltzman constant (5.67×10^{-8}wm^{-1} K^{-4}) and T_a and T_s are the air and surface temperature (K), respectively. ε_a was calculated from T_a using the following formula (Idso and Jackson, 1969):

$$\varepsilon_a = 1-0.261^*\exp\left[-7.77^*10^{-4}*(273-T_a)^2\right] \quad (12)$$

The surface emissivity (ε_a) was estimated according to the approach proposed by Jin and Liang (2006):

$$\varepsilon_s = 0.4587^*\varepsilon_{31} + 0.5414^*\varepsilon_{32} \quad (13)$$

where ε_{31} and ε_{32} are the spectral emissivity in MODIS bands 31 and 32, which are part of LST products.

We used the 1 km 16-day MCD43B3 Version-5 MODIS/Terra + Aqua BRDF/Albedo product. The actual surface albedo was obtained by adding 50% of the black-sky albedo and 50% of the white-sky albedo. Similarly, each 16-day composite albedo was assigned to the corresponding 16 daily periods. For the details of MODIS albedo products' algorithm and validation, interested readers are suggested to refer to Schaaf et al. (2002) and Jin et al. (2003a,b).

3.2.4. Collection5 MOD17 GPP

The old Collection4 gross primary production products were found to have considerable errors due to the problems in the inputs (Zhao et al., 2005). Zhao et al (2005) rectified these problems by improving the data process methods and modifying parameters the algorithm used, which resulted in improved Collection5 MOD17 estimates. Collection5 MOD17 8-day GPP data for the conterminous U.S. from January 2004 to December 2005 were obtained from http://www.ntsg.umt.edu. Monthly and annual GPP averages were derived by summing up each 8-day period to get monthly values for the period of 2004–2005.

Table 1
Eddy flux sites used in this study.

Site	Latitude	Longitude	Vegetation structure	Vegetation type	Year	References
ARM Oklahoma, OK (ARM)	36.60	−97.49	Winter wheat, some pasture and summer crops	Croplands	2003–2006	Sims and Bradford (2001)
Audubon Research Ranch, AZ (ARR)	31.59	−110.51	Desert grasslands	Grasslands	2003–2006	
Bartlett Experimental Forest, NH (BEF)	44.06	−71.29	Temperate northern hardwood forest dominated by American beech, red maple, paper birch, and hemlock	Deciduous broadleaf forest	2003–2006	Jenkins et al. (2007)
Blodgett Forest, CA (BF)	38.90	−120.63	Mixed evergreen coniferous forest dominated by ponderosa pine (N70%)	Evergreen broadleaf forest	2003–2006	Misson et al. (2007)
Bondville, IL (BO)	40.00	−88.29	Annual rotation between corn (C4) and soybeans (C3)	Croplands	2003–2006	Hollinger et al. (2005)
Brookings, SD(Bro)	44.35	−96.84	Temperate grassland	Grasslands	2003–2006	
Fort Peck, MT (FP)	48.31	−105.10	Grassland	Grasslands	2003–2006	
Freeman Ranch Mesquite Juniper, TX (FRM)	29.94	−97.99	Grassland in transition to an Ashe juniper dominated woodland	Woody savannas	2003–2006	Kjelgaard et al. (2008)
Goodwin Creek, MS (GC)	34.25	−89.97	Temperate grassland	Croplands	2003–2006	
Harvard Forest EMS Tower, MA (HFE)	42.53	−72.17	Temperate deciduous forest dominated by red oak, red maple, black birch, white pine, and hemlock	Mixed forests	2003–2006	Urbanski et al. (2007)
Howland Forest, ME (HF)	45.20	−68.72	Boreal—northern hardwood transitional forest consisting of hemlock-spruce-fir, aspen-birch, and hemlock-hardwood mixtures	Mixed forests	2003–2006	Hollinger et al. (1999, 2004)
Kennedy Space Center-Scrub Oak, FL (KSC)	28.61	−80.67	Scrub-oak palmetto dominated by schlerophyllous evergreen oaks and the Saw Palmetto *Serenoa repens*	Open shrublands	2003–2006	Dore et al. (2003)
Lost Creek, WI (LC)	46.08	−89.98	Alder-willow deciduous wetland	Mixed forests	2003–2006	Yi et al. (2004)
Mead Irrigated Continuous, NE (MIC)	41.17	−96.48	Continuous maize	Croplands	2003–2006	Verma et al. (2005)
Mead Irrigated Rotation, NE (MIR)	41.16	−96.47	Maize–soybean rotation	Croplands	2003–2006	Verma et al. (2005)
Mead Rainfed, NE (MR)	41.18	−96.44	Maize–soybean rotation	Croplands	2003–2006	Verma et al. (2005)
Metolius Intermediate, OR (MI)	44.45	−121.55	Temperate coniferous forest dominated by *Pinus ponderosa*, *Purshia tridentate*, and *Arctostaphylos patula*	Evergreen needleleaf forest	2003–2006	Law et al. (2003) Irvine et al. (2007)
Missouri Ozark, MO (MO)	38.74	−92.20	Oak hickory forest	Deciduous broadleaf forest	2003–2006	Gu et al. (2007)
Niwot Ridge, CO (NR)	40.03	−105.55	Subalpine coniferous forest dominated by subalpine fir, engelmann spruce, and lodgepole pine	Evergreen needleleaf forest	2003–2006	Monson et al. (2002)
Mize, FL (MI)	29.76	−82.24	Pine plantation dominated by *Pinus elliottii*	Savannas	2003–2006	Powell et al. (2008)
Morgan Monroe State Forest, IN (MMS)	39.32	−86.41	Mixed hardwood deciduous forest dominated by sugar maple, tulip poplar, sassafras, white oak, and black oak	deciduous broadleaf forest	2003–2006	Sims et al. (2008)
North Carolina Clearcut, NC (NCC)	35.81	−76.71	15-year-old loblolly pine (*Pinus taeda*) plantation	Mixed forests	2003–2006	
Rosemount G19, MN (RG)	44.72	−93.09	Corn–soybean annual rotation	Croplands	2003–2006	Baker and Griffis (2005)
Sky Oaks Young stand, CA (SOY)	33.38	−116.64	Chaparral (Mediterranean-type ecosystems)	Closed shrubland	2003–2006	Lipson et al. (2005)
Tonzi Ranch, CA (TR)	38.43	−120.97	Oak savanna, grazed grassland dominated by blue oak and grasses	Woody savannas	2003–2006	Ma et al. (2007)
Vaira Ranch, CA (VR)	38.41	−120.95	Grazed C3 grassland opening in a region of oak/grass savanna	Grasslands	2003–2006	Xu and Baldocchi (2004)
Walnut River, KS (WR)	37.52	−96.44	C3/C4 mixed grassland, tallgrass prairie	Grasslands	2003–2006	Chen et al. (2003)
Wind River, WA (WR)	45.82	−121.95	Old coniferous, temperate rainforest, evergreen forest dominated by Douglas fir, western hemlock	Evergreen needleleaf forest	2003–2006	Falk et al. (2008)

The units of latitude and longitude are in decimal degrees.
The names in the parentheses are abbreviations of flux sites.

4. Verification at the eddy flux tower sites

4.1. ET validation

We verified the daily latent heat (ET) estimates using eddy flux measurements in 2006. For each explanatory variable derived from MODIS data, we used the values averaged within the 7×7 km area surrounding each flux tower to represent the values of the tower site.

ANNs performance varied between flux sites (Fig. 2 (A)). The lowest R^2 of 0.51 occurred at ARM SGP Main and the highest R^2 of 0.86 occurred at Bondville, both within croplands, which means ET on croplands has high variations. R^2 is also below 0.6 at Mead Rainfed. At these sites, the measurements were available in the first 136 days of 2006, when vegetation is not in the most active growth period. This may be the reason for the relative poor performance of model prediction. At Kennedy Space Center and Wind River Crane, R^2 are only 0.56 and 0.55, respectively. By checking the ANNs at these sites, we found the remotely-sensed training datasets are limited due to their low quality in 2004 and 2005. This weakened the predictability of the ANNs. In general, ANNs trained with more data worked generally better than the ANNs trained with less. To have enough training data is important. We concluded that, given the

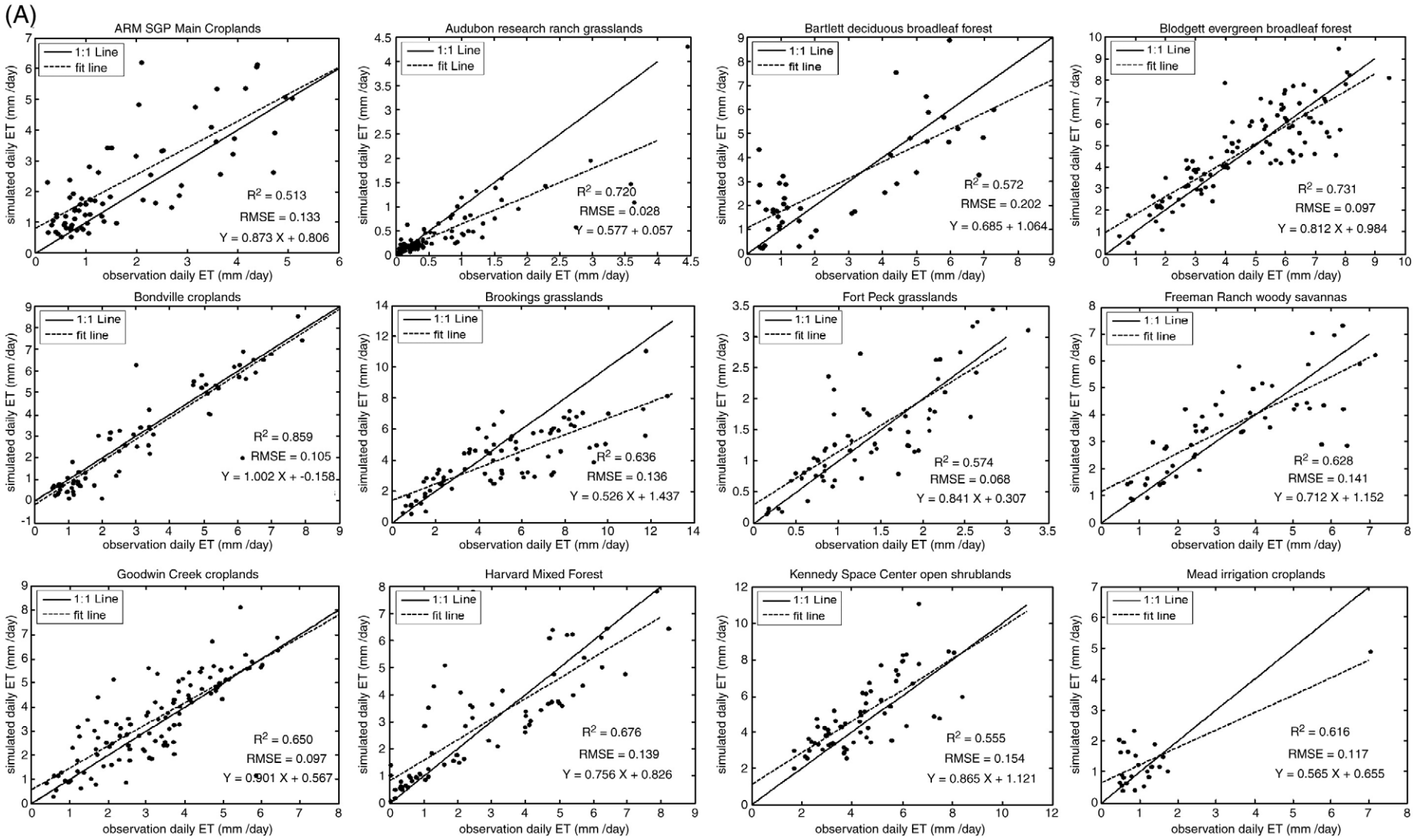

Fig. 2. Observed and estimated daily ET (mm/ day) (A), and WUE (g C g^{-1} H_2O) (B) for each AmeriFlux site in 2006. Site information is given in Table 1.

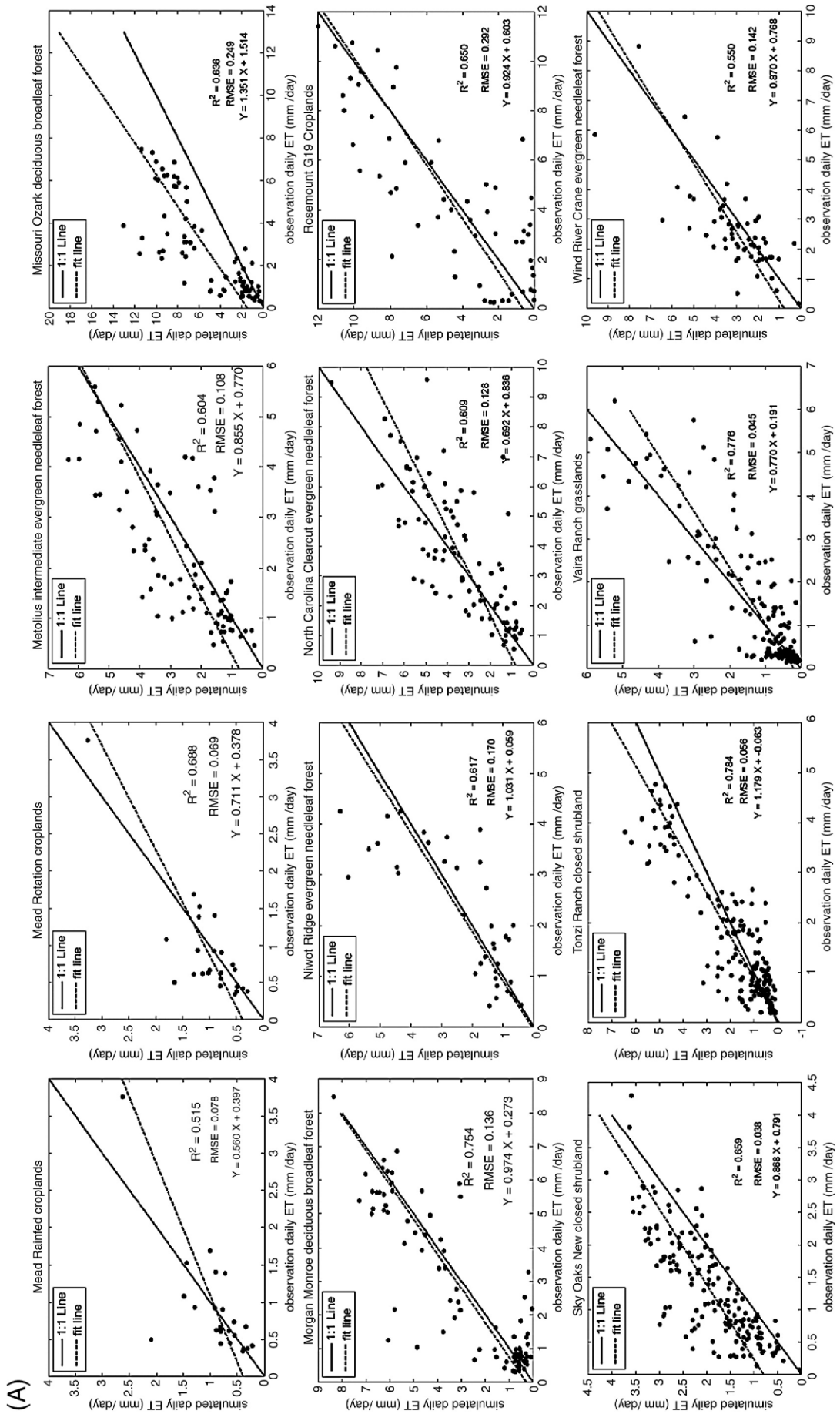

Fig. 2 (*continued*).

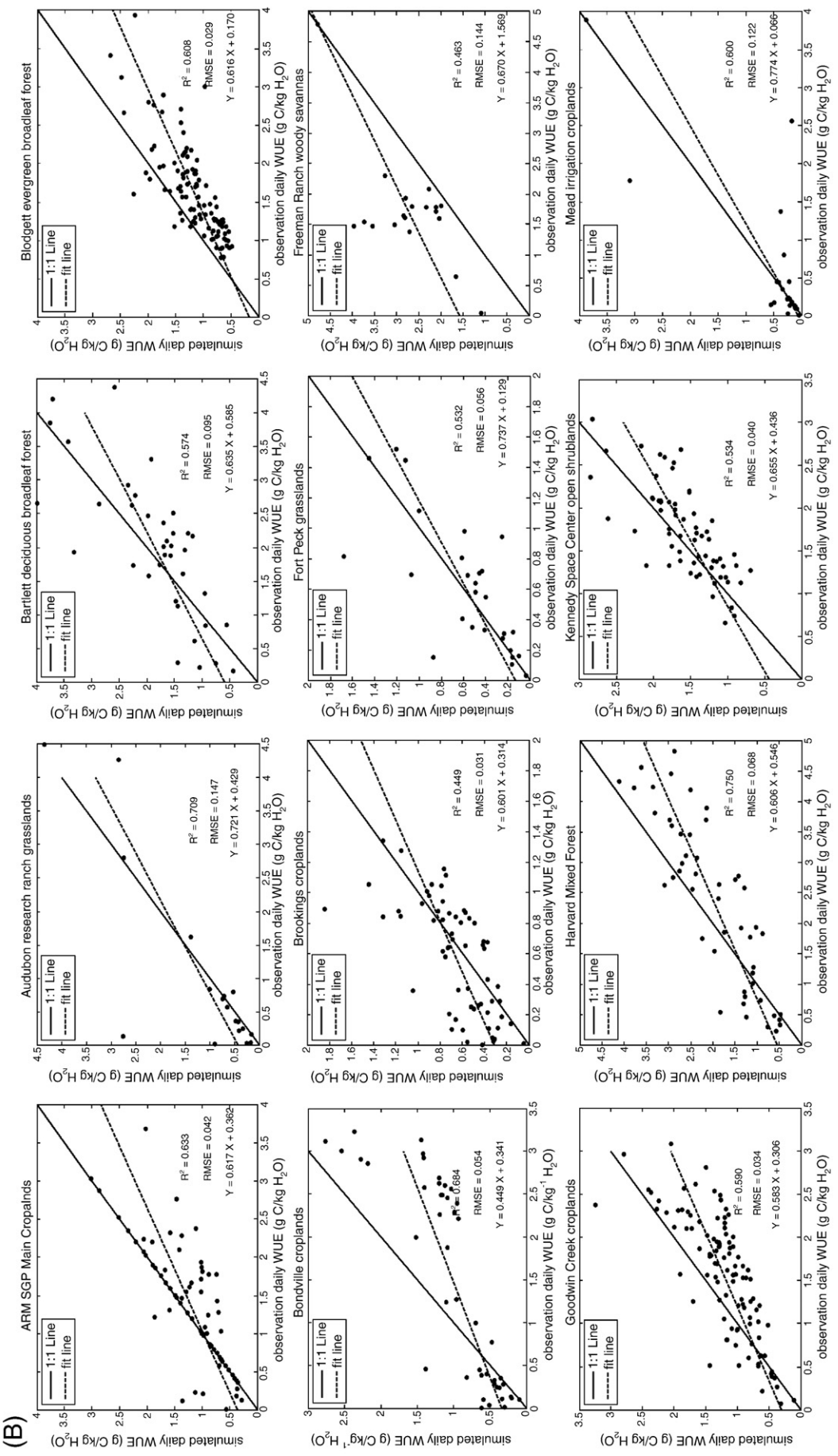

Fig. 2 (*continued*).

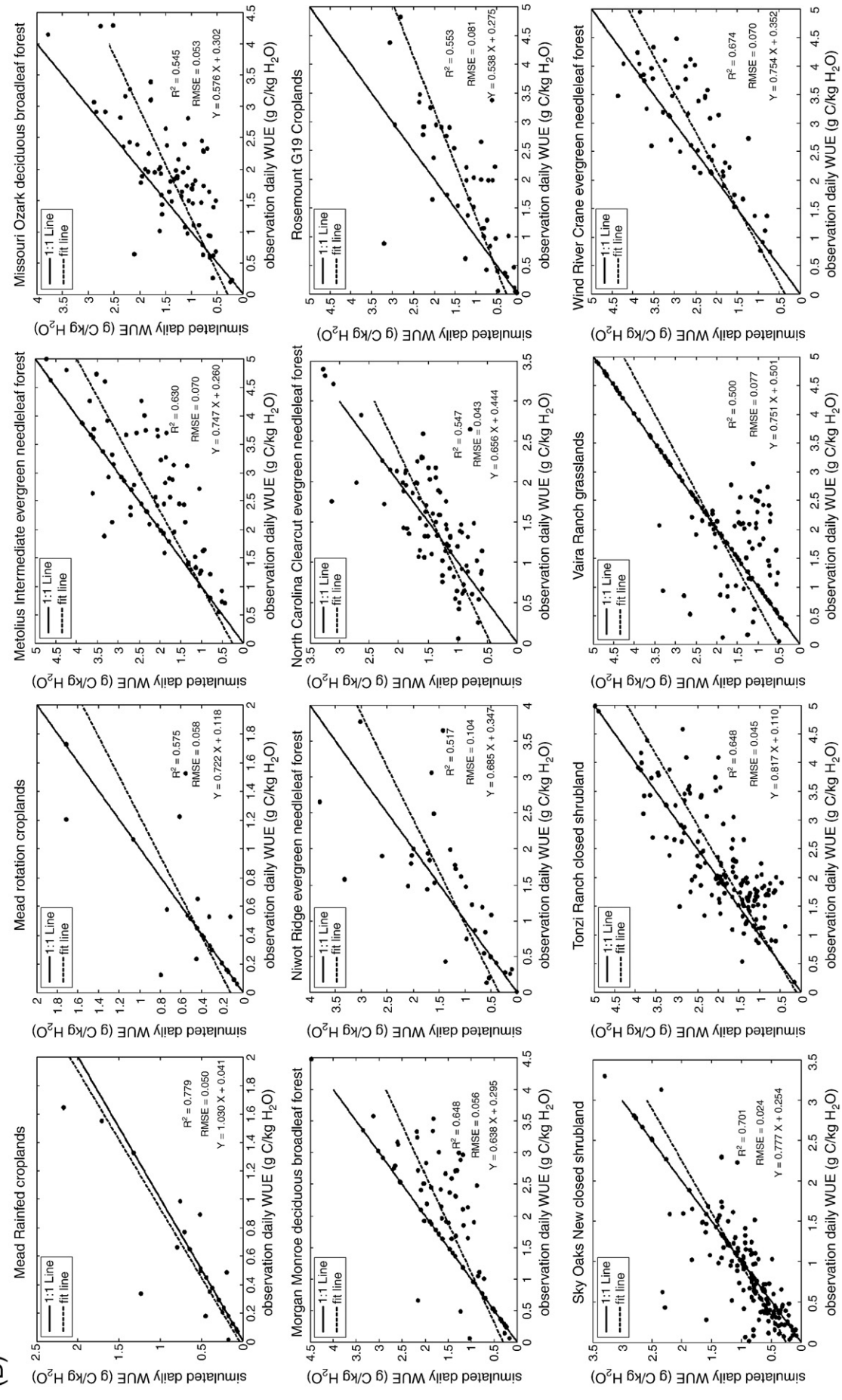

Fig. 2 (*continued*).

heterogeneity of the AmeriFlux data and the simplicity of the model inputs, our ANNs model performance is satisfactory.

4.2. WUE validation

We also verified the daily WUE estimates using eddy flux measurements in 2006. The site-level WUE measurements were calculated by the ratio of GPP to latent heat. The Level 4 product of eddy flux measurements consists of two types of GPP data, including standardized (GPP_st) and original (GPP_or) GPP (AmeriFlux, 2007). Both GPP_st and GPP_or were filled using the Marginal Distribution Sampling (MDS) method (Reichstein et al., 2005) and the Artificial Neural Network (ANN) method (Papale and Valentini, 2003). The ANN method is generally better than the MDS method (Moffat et al., 2007). Therefore, we used the gap-filled GPP data based on the ANN method. For each site, if the percentage of the number of missing values to the total number of measurements for GPP_st was lower than that for GPP_or, we selected GPP_or; otherwise, we used GPP_st.

Comparisons between estimates with ANNs and eddy flux data indicate that performance of WUE estimates at site level is slightly poorer than ET estimates (Fig. 2 (B)). The lowest R^2 of 0.46 occurred at Freeman ranch site and the highest R^2 of 0.75 occurred at Harvard site. It is partially due to the uncertainties introduced by using MODIS products. Overall, WUE estimates are best for forests, grasslands and shrublands. WUE estimates show large variations for croplands. Similar to ET, the amount of training data is important to the performance of the ANNs.

Many factors may bring negative effects to the ET estimation algorithm (Mu et al., 2007). The relative low performance of the ANNs at some sites may results from: (1) biases in the meteorological data. Although the conterminous US has a dense weather station network, the reanalysis datasets still contain uncertainties (Kistler et al., 2001; Zhao et al., 2006). The spatial interpolation scheme which doesn't consider the terrain may also lead to errors in the forcing meteorological data; (2) limitations in the MODIS products. Some remotely-sensed variables, such as LAI and LST, have large variations, especially for the daily products (Wan et al., 2002). Although the gap-filling method can provide more available forcing data, their quality is likely poorer than the direct observations. Moreover, the simple LUE scheme used by the GPP algorithm may not work well when some other factors become more important in the carbon assimilation, which will in turn deteriorate the WUE estimate; (3) effect of water redistribution. Precipitation will be redistributed as a result of topography or the water management. Two neighbor pixels with almost the same explanatory variables may have the huge difference in ET due to the difference in water bodies' area. (4) Issues are with the ANNs itself. The effect of the lack of training data has been discussed before. Some explanatory variables, such as soil moisture, are important for estimating ET. However, MODIS can't directly measure soil moisture. Although its effect is implicitly considered in the NDWI and LST, the ANNs will most likely suffer the loss of accuracy under some circumstances.

5. Results and discussion

5.1. Spatiotemporal patterns of ET

Aggregated daily ET estimates for each month in 2004 shows a large spatial variability (Fig. 3). Because remote sensing data required by ANNs were not always available in a given composite period or ANNs were failed (when EF>1 or EF <0) due to limited training datasets, the missed EF or ET was assigned with the values from the most adjacent grid cells. To show the quality of the model output data, we defined the quality flag as the fraction of daily data with EF between 0 and 1. The quality flag maps for each month in 2004 were presented in Fig. 4.

The ANNs trained at the AmeriFlux sites generally captured the expected spatiotemporal patterns of ET, with a maximum ET of 1554 mm/yr and 1443 mm/yr, an average of 529 mm/yr and 533 mm/yr in 2004 and 2005, respectively. Temporally, the majority of the

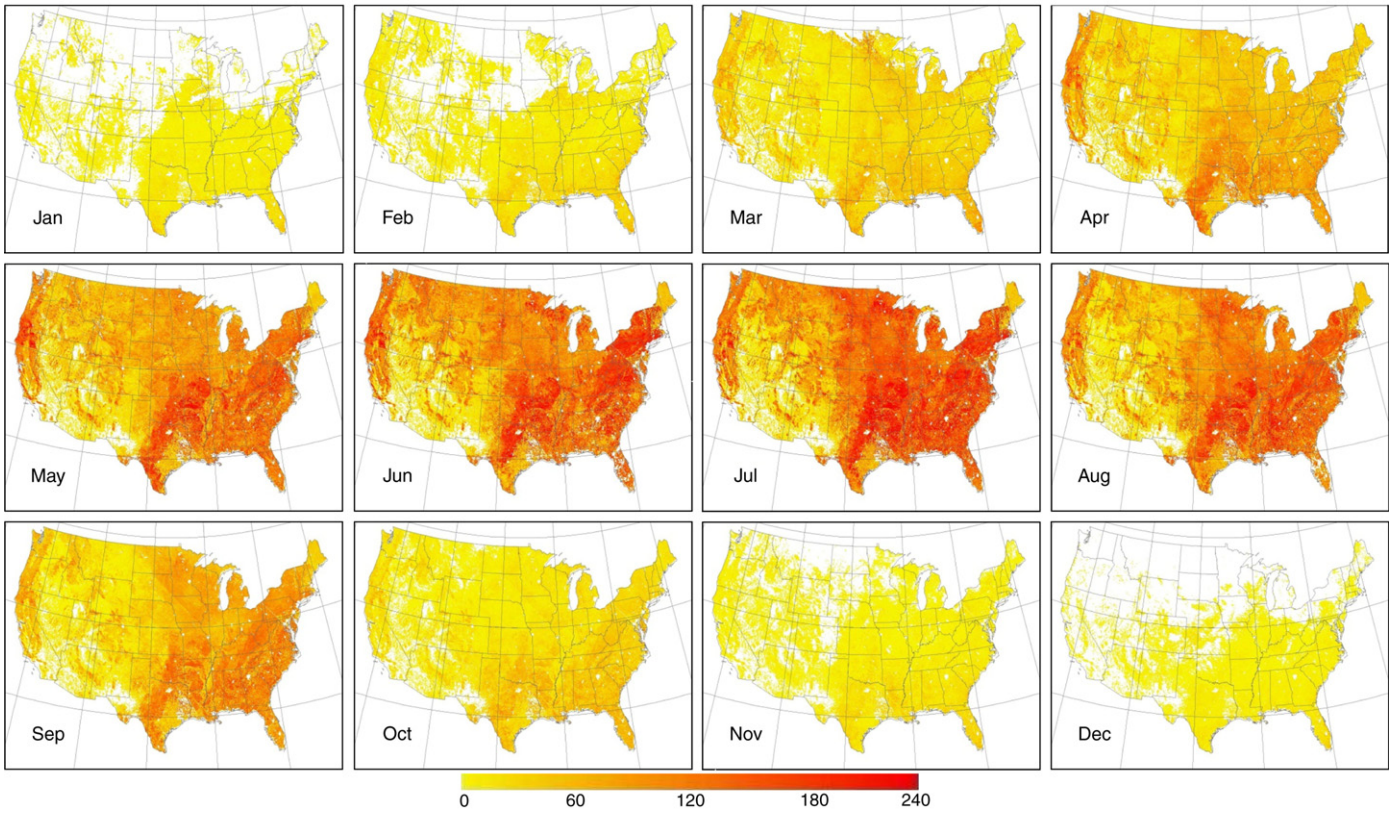

Fig. 3. Predicted monthly ET for the conterminous U.S. from January through December in 2004. Units are in mm/month.

conterminous U.S. has very low ET (Fig. 3) in winter months (December–February) due to low available energy, temperature, and stomatal conductance. The associated data quality is also very poor and most of northern regions even have no values since most remotely-sensed variables, such as LAI, NDVI and NDWI are in bad quality due to snow cover (Fig. 4). ET magnitude went to the highest level in summer months (June–August) because of high precipitation, dense vegetation, and intensive radiation. In fall period (September–November), ET dropped as vegetation senesced and radiation declines (Fig. 3). Moreover, we found that pixels under slight dryness (explain later) have a higher ET than neighbor pixels which have the same land cover type and are not under drought.

Spatially, ET increased from south to north and from the coast to the interior, reflecting variations in rainfall, available energy, and temperature. ET rates also demonstrate a high correlation with the land cover type. In particular, the quality of training data for ANNs is limited for shrublands. There are many places lacking of quality data in open and closed shrublands at the regional scale (Fig. 4). As expected, deciduous broadleaf forest have the highest ET values which are 644 and 652 mm/yr in 2004 and 2005, respectively; open/closed shrublands, which are mainly located in dry areas with short growing seasons, have the lowest ET, which are 247 and 287 mm/yr in 2004 and 2005, respectively. The ET for evergreen needleleaf or broadleaf forest, mixed forest, savannas, grasslands and croplands lies between the two extremes. ET of croplands is generally higher than that of grasslands, which may be due to irrigation in croplands.

5.2. Water-use efficiency analysis

5.2.1. Spatial and temporal patterns of water-use efficiency

To date, numerous studies on WUE have focused on analyzing its relationship with environment factors, such as elevated CO_2, stand age, and vegetation types at a leaf level (Collatz et al., 1991; Jarvis, 1995; Medrano et al., 2009), rather than on an ecosystem scale. Here we aggregated spring (March–May), summer (June–August) and fall (September–November) seasons' ecosystem-level WUE in 2004 and 2005 from our ET estimates (Fig. 5). We excluded winter seasons because plants are in inactive growth periods. Abnormally high values of WUE (greater than 5 g C kg^{-1} H_2O) were treated as no value. By visual interpretation of Fig. 5, the plant functional type is an important factor to determine the spatial pattern of ecosystem-level WUE. The seasonal mean WUE values for each ecosystem are listed in Table 2. The gradient WUE from low to high is grassland, cropland, shrubland and then forests. Evergreen broad-leaf forest has the highest WUE, intermediate at evergreen needle-leaf forest and lowest at the deciduous needle/broad leaf forest. Mixed forest has the average WUE among forest ecosystem types.

Majority of ecosystems has relative lower WUE in summer seasons than in fall seasons (Table 2), which means water loss rate is higher than the increase rate of carbon assimilation. It seems that plants tend to grow fast even with a lower WUE during summer. This may be due to that the more soil water is available to plant as summer precipitation tends to be higher. The distinct differences in WUE among various ecosystems and their seasonal variations might be determined by both inherent biological characteristics and external environmental conditions.

5.2.2. Relationship between water use efficiency and drought condition

Understanding the effects of water availability on ecosystem carbon assimilation is important to quantifying carbon budget of ecosystems, especially in drought areas. Carbon uptake of ecosystems is generally thought to decrease under the water-limited environment (Running and Hunt, 1993; Hunt et al., 1996). Here we analyzed WUE responses of each ecosystem to drought. Drought monitor summary maps from UNL (http://drought.unl.edu/dm/dmshps_archive.htm) were used to represent the intensity and spatial distribution of

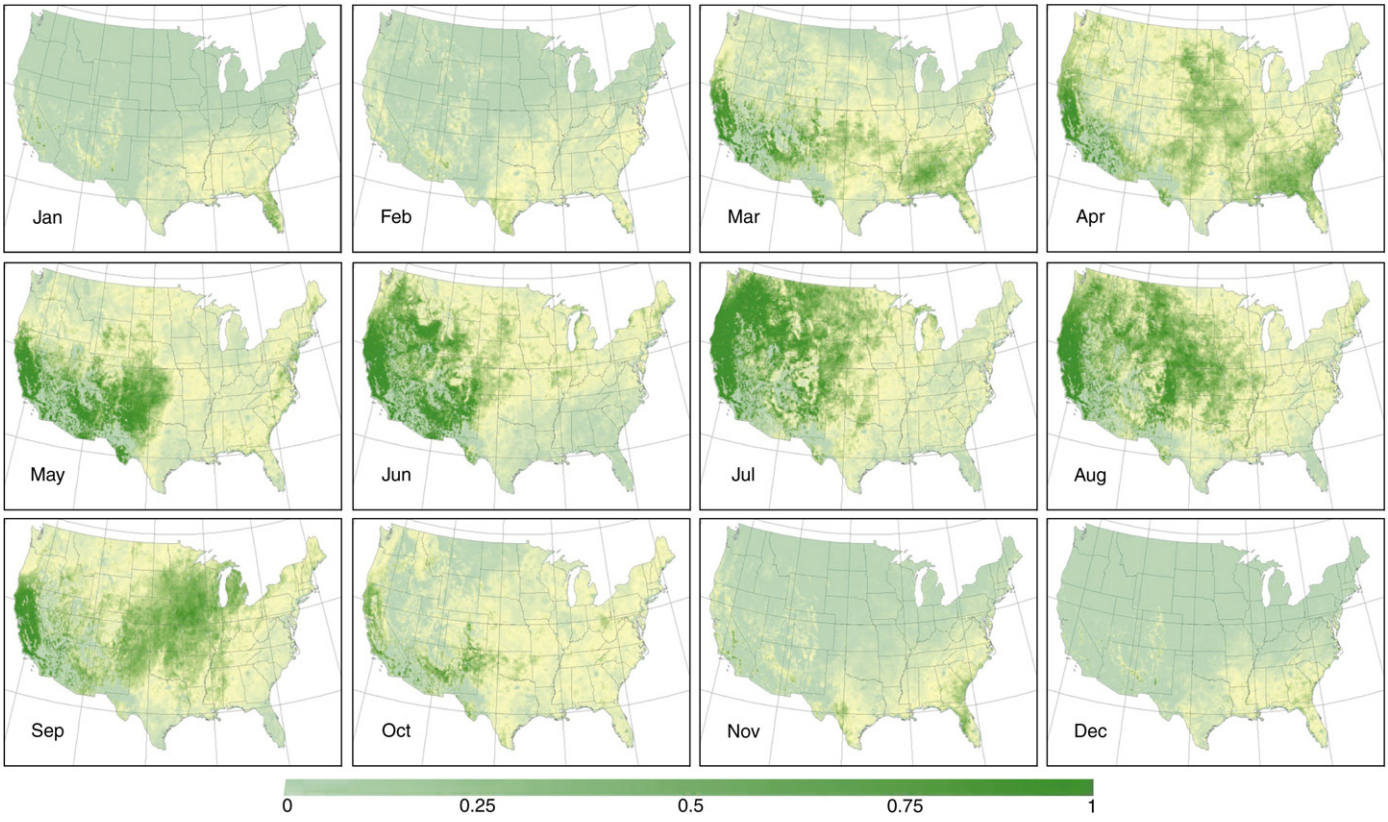

Fig. 4. Monthly quality flag maps for the conterminous U.S. from January through December of 2004.

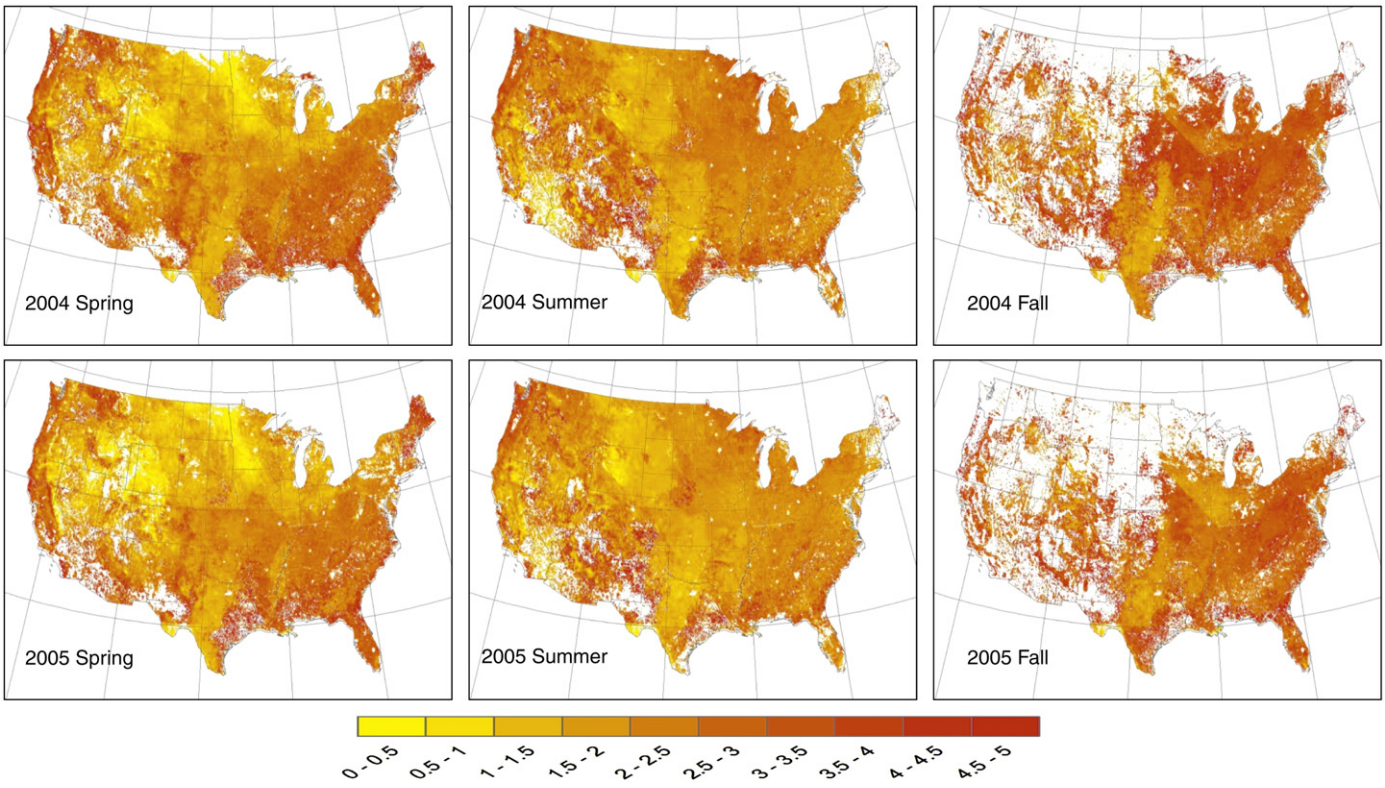

Fig. 5. Spring, summer and fall seasonal water-use efficiency (g C g^{-1} H_2O) for the conterminous U.S. in 2004 and 2005.

drought. The maps are weekly updated for the whole of the U.S. and drought is categorized into five levels: abnormally dry (D0), moderate (D1), severe (D2), extreme (D3) and exceptional (D4) drought according to five key indicators and numerous supplementary indicators. D0 is used for areas showing dryness but not yet in drought, or for areas recovering from drought. To make the drought maps and WUE products have the same time step, we generated weekly WUE data using daily ET and weekly GPP products. The required weekly GPP were made from disaggregating one or two 8-day standard MODIS GPP products.

Two drought maps for the first two weeks in August 2004 and 2005 were used in our analysis (Fig. 6 (A) and (B)). In 2004, most of drought happened in west and southwestern grasslands and shrublands (Fig. 6 (A)). On the contrary, drought mainly took place in the Midwest grasslands and croplands and southern forests in 2005 (Fig. 6 (B)). These periods were selected because: (1) August is in the active growth period for most ecosystems; (2) these two years have large differences in drought area and intensity, providing a good opportunity to study ecosystems' WUE responses. To test WUE responses to dryness for each ecosystem, seventeen circle study regions with a radius of 80 km were further chosen (Fig. 6). Two factors were used to decide the locations of the regions: (1) there is one interested ecosystem type dominating the region and (2) there is an obvious difference in drought intensity between these two years. The properties of these regions are listed in Table 3. We did not consider evergreen broadleaf and deciduous needle leaf forests here due to their small fractions in the region. Although each ecosystem has somewhat random WUE values under different drought intensities, there is a pattern: ecosystem WUE showed a biphasic trend with the drought intensity, which can be found in Table 3. Specifically, WUE tended to increase when drought initially happened and increased progressively from abnormally dry (D0) to moderate (D1) level. However, WUE decreased as drought's intensity progressed from moderate to severe (D2), extreme (D3) or even exceptional (D4). More interestingly, WUE values were even lower under extreme drought (D3) than those under no dryness, which is shown by the results in the 4th, 7th and 17th regions. This is not consistent with current models, which usually assume a monotonously increase water-use efficiency under the assumption of stomatal regulation of water losses with slight photosynthetic reductions (Flexas and Medrano, 2002). The two-stage pattern identified in our study has been also observed by Reichstein et al. (2002) and Yu et al (2008) at eddy flux sites. They believed the decline in WUE under drought conditions is most likely due to impairment of electron transport and carboxylation capacity and thus reducing carbon assimilation capacities and active leaf area (Reichstein et al., 2002, 2003; Harley and Tenhunen, 1991). Our results also suggest that the two-stage pattern concerning WUE should be considered in modeling drought effect on plant photosynthesis and carbon cycling at regional scales.

Table 2
Mean water use efficiency (g C kg^{-1} H_2O) in spring, summer and fall seasons for each ecosystem type.

	2004 spring	2004 summer	2004 fall	2005 spring	2005 summer	2005 fall
Evergreen needle leaf forest	2.2	2.2	3.0	1.9	2.1	3.1
Evergreen broadleaf forest	3.2	2.6	3.1	3.1	2.7	3.3
Deciduous needle leaf / broadleaf forest	2.4	1.9	2.6	2.2	1.9	2.8
Mixed forest	2.5	2.3	2.8	2.6	2.1	2.9
Open/closed shrubland	1.9	2.3	2.8	1.9	2.2	2.8
Savannas/woody savannas	2.5	2.1	2.7	2.5	2.0	2.8
Grassland	1.3	1.6	2.0	1.5	1.6	2.5
Croplands	1.8	2.1	2.8	1.7	1.8	2.6

6. Summary and conclusion

Using a combination of tower-based observations from 28 AmeriFlux sites, artificial neural networks, and remotely-sensed

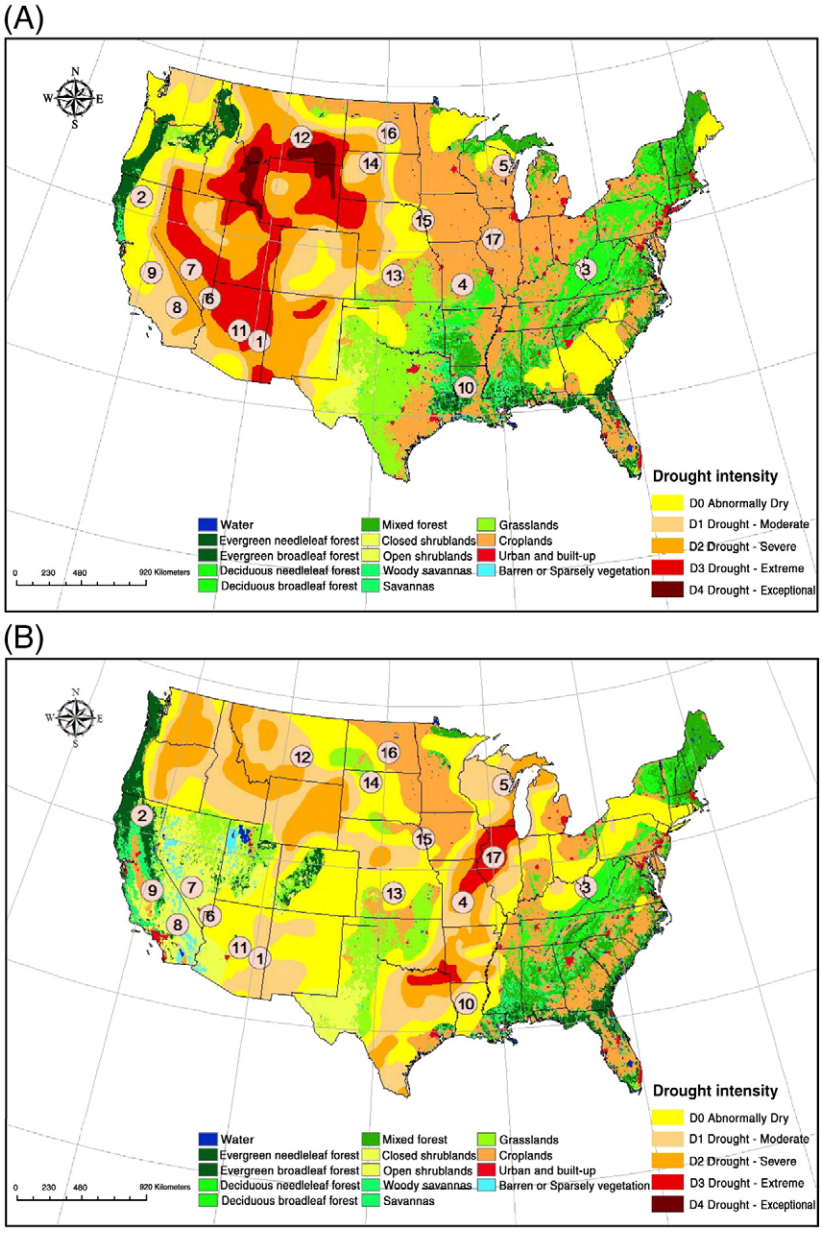

Fig. 6. Drought level distribution maps in 2004(A) and 2005 (B) and the experiment regions (denoted with numbers).

Table 3
Responses of plants' water-use efficiency to drought in the selected experiment regions in Fig. 6. D0, D1,D2, D3and D4 represent abnormally dry, moderate, severe, extreme and exceptional drought, respectively.

The number of study region	Dominant ecosystem type	Drought level for the first two weeks in August 2004	Average WUE (g C kg^{-1} H_2O)	Drought level for the first two weeks in August 2005	Average WUE (g C kg^{-1} H_2O)
1	Evergreen needleleaf forest	D3	4.23	D0	4.50
2	Evergreen needleleaf forest	D1	5.26	No drought	4.70
3	Deciduous broadleaf forest	No drought	5.31	D1	5.91
4	Deciduous broadleaf forest	No drought	5.78	D3	3.79
5	Deciduous broadleaf forest	D0	7.35	D2	5.72
6	Open/closed shrubland	D3	2.95	D0	6.55
7	Open/closed shrubland	D3	2.46	No drought	3.77
8	Open/closed shrubland	D1	2.73	No drought	1.79
9	Savannas/woody savannas	D0	6.48	No drought	4.08
10	Savannas/woody savannas	No drought	5.19	D1	5.40
11	Savannas/woody savannas	D3	4.33	D0	5.54
12	Grasslands	D3	4.85	D0	5.92
13	Grasslands	No drought	3.19	D0	6.27
14	Grasslands	D2	4.29	No drought	6.36
15	Croplands	D0	7.04	No drought	5.58
16	Croplands	D0	5.06	No drought	4.54
17	Croplands	No drought	6.85	D3	4.46

environmental data, we developed a predictive EF model. Daily ET was then estimated from available energy and the predicted EF. We applied the model to the conterminous U.S. using the interpolated 4 km gridded meteorological datasets and the MODIS data to provide a 2-year, daily land surface ET. The spatiotemporal ET patterns are generally reasonable and site-level validation demonstrated the model is able to capture the ET variation. Besides the need to have plenty eddy flux data for training ANNs, the quality of MODIS input data and limitation of ANNs limit the accuracy of the regional estimates of ET.

Together with the MODIS GPP products, estimated ET were used to derive WUE on the continental scale. Our continental scale WUE analysis suggests that the "classical pure stomatal control" hypothesis should be modified. In mild and moderate dry areas, the increasing in WUE reflects plants' physiologic acclimation to water stresses. However, under severe and exceptional drought condition, WUE will decrease. When a certain drought condition is reached, disability and impairment to plant photosynthetic apparatus may occur. Our analysis suggests that more sophisticated water-use efficiency mechanism should be further identified and considered in ecosystem water and carbon modeling. In addition, this study provides a new way to quantify daily ET for various ecosystems at large spatial scales.

Acknowledgement

This study was funded by the National Science Foundation (NSF) and the Department of Energy (DOE). We thank the principal investigators of the MODIS data products and AmeriFlux network. We also thank the group of Prof. Shunlin Liang at University of Maryland to provide MODIS-based Photosynthetically Active Radiation (PAR) data. Computing support was provided by the Rosen Center for Advanced Computing at Purdue University.

References

AmeriFlux, 2007. AmeriFlux Network http://public.ornl.gov/ameriflux/

Baldocchi, D. D., & Harley, P. C. (1995). Scaling carbon dioxide and water vapour from leaf to canopy in a deciduous forest. II. Model testing and application. *Plant, Cell and Environment*, *18*, 1157−1173.

Baldocchi, D. D. (1997). Measuring and modeling carbon dioxide and water vapor exchange over a temperate broad-leaved forest during the 1995 summer drought. *Plant, Cell and Environment*, *20*, 1108−1122.

Baldocchi, D. D., & Wilson, K. B. (2001). Modelling CO2 and water vapor exchange of a temperate broadleaved forest across hourly to decadal time scales. *Ecological Modelling*, *142*, 155−184.

Baldocchi, D., Falge, E., Gu, L. H., Olson, R., Hollinger, D., Running, S., et al. (2001). FLUXNET: A new tool to study the temporal and spatial variability of ecosystem-scale carbon dioxide, water vapor, and energy flux densities. *Bulletin of the American Meteorological Society*, *82*, 2415−2434.

Baldocchi, D. (2003). Assessing the eddy covariance technique for evaluating carbon dioxide exchange rates of ecosystems: Past, present and future. *Global Change Biology*, *9*, 479−492.

Baldocchi, D., Verma, S. B., & Anderson, D. E. (2003). Canopy photosynthesis and water-use efficiency in a deciduous forest. *Journal of Applied Ecology*, *24*(1), 251−260.

Bastiaanssen, W. G. M., Menenti, M., Feddes, R. A., & Holtslag, A. A. M. (1998). A remote sensing surface energy balance algorithm for Land (SEBAL): Part 1. Formulation. *Journal of Hydrology*, 212−213.

Bastiaanssen, W. G. M., Pelgrum, H., Wang, J., Ma, Y., Moreno, J., Roerink, G. J., et al. (1998). The surface energy balance algorithm for land (SEBAL): Part 2. Validation. *Journal of Hydrology*, *212–213*, 213−229.

Baker, J. M., & Griffis, T. J. (2005). Examining strategies to improve the carbon balance of corn/soybean agriculture using eddy covariance and mass balance techniques. *Agricultural and Forest Meteorology*, *128*(3–4), 163−177.

Berk, A., Bernstein, L. S., Anderson, G. P., Acharya, P. K., Robertson, D. C., Chetwynd, J. H., et al. (1998). MODTRAN cloud and multiple scattering upgrades with application to AVIRIS. *Remote Sensing of Environment*, *65*, 367−375.

Carlson, T. N., Gillies, R. R., & Perry, E. M. (1994). A method to make use of thermal infrared temperature and NDVI measurements to infer surface soil water content and fractional vegetation cover. *Remote sensing Reviews*, *9*, 161−173.

Carlson, T. N., Gillies, R. R., & Schmugge, T. J. (1995). An interpretation of methodologies for indirect measurement of soil water content. *Agricultural and Forest Meteorology*, *77*, 191−205.

Carlson, T. N., Capehart, W. J., & Gillies, R. R. (1995). A new look at the simplified method for remote sensing of daily evapotranspiration. *Remote Sensing of Environment*, *54*, 161−167.

Ceccato, P., Flasse, S., Tarantol, S., Jacquemoud, S., & Gregoire, J. -M. (2001). Detecting vegetation leaf water content using reflectance in the optical domain. *Remote Sensing of Environment*, *77*, 22−33.

Centritto, M., Lucas, M. E., & Jarvis, P. G. (2002). Gas exchange, biomass, whole-plant water-use efficiency and water uptake of peach (*Prunus persica*) seedlings in response to elevated carbon dioxide concentration and water availability. *Tree Physiology*, *22*, 699−706.

Chen, F., Yates, D. N., Hagi, H., LeMone, M. A., Ikeda, K., & Grossman, R. L. (2003). Land surface heterogeneity in the cooperative atmosphere surface exchange study (CASES-97). Part I: Comparing modeled surface flux maps with surface-flux tower and aircraft measurements. *Journal of Hydrometeorology*, *4*(2), 196−218 April.

Cleugh, H. A., & Dunin, F. X. (1995). Modelling sensible heat fluxes from a wheat canopy: An evaluation of the resistance energy balance method. *Journal of Hydrology*, *164*, 127−152.

Cleugh, H. A., Leuning, R., Mu, Q., & Running, S. W. (2007). Regional evaporation estimates from flux tower and MODIS satellite data. *Remote Sensing of Environment*, *106*, 285−304. doi:10.1016/j.rse.2006.07.007

Collatz, G. J., Ball, J. T., Grivet, C., & Berry, J. A. (1991). Physiological and environmental regulation of stomatal conductance, photosynthesis and transpiration: A model that includes a laminar boundary layer. *Agricultural and Forest Meteorology*, *54*, 107−136.

Crago, R. D. (1996). Comparison of the evaporative fraction and the Priestley–Taylor a for parameterizing daytime evaporation. *Water Resources Research*, *32*(5), 1403−1409.

Crago, R., & Brutsaert, W. (1996). Daytime evaporation and the self-preservation of the evaporative fraction and the Bowen ratio. *Journal of Hydrology*, *178*, 241−255.

Dore, S., Hymus, G. J., Johnson, D. P., Hinkle, C. R., Valentini, R., & Drake, B. G. (2003). Cross validation of open-top chamber and eddy covariance measurements of ecosystem CO2 exchange in a Florida scrub-oak ecosystem. *Global Change Biology*, *9*, 84−95.

Falk, M., Wharton, S., Schroeder, M., Ustin, S., & Paw, U. K. T. (2008). Flux partitioning in an old-growth forest: seasonal and interannual dynamics. *Tree Physiology*, *28*, 509−520.

Fensholt, R., & Sandholt, I. (2003). Derivation of a shortwave infrared water stress index from MODIS near- and shortwave infrared data in a semiarid environment. *Remote Sensing of Environment*, *87*, 111−121.

Fisher, J. B., Tu, K., & Baldocchi, D. D. (2008). Global estimates of the land–atmosphere water flux based on monthly AVHRR and ISLSCP-II data, validated at 16 FLUXNET sites. *Remote Sensing of Environment*, *112*, 901−919.

Flexas, J., & Medrano, H. (2002). Drought-inhibition of photosynthesis in C3 plants: Stomatal and non-stomatal limitations revisited. *Annals of Botany*, *89*, 183−189.

Friedl, M. A., McIver, D. K., Hodges, J. C. F., Zhang, X. Y., Muchoney, D., Strahler, A. H., et al. (2002). Global land cover mapping from MODIS: Algorithms and early results. *Remote Sensing of Environment*, *83*, 287−302.

Gao, B. C. (1996). NDWI — a normalized difference water index for remote sensing of vegetation liquid water from space. *Remote Sensing of Environment*, *58*, 257−266.

Gao, Y. C., Long, D., & Li, Z. L. (2008). Estimation of daily actual evapotranspiration from remotely sensed data under complex terrain. *International Journal of Remote Sensing*, *29*(11), 3295−3315.

Gillies, R. R., & Carlson, T. N. (1995). Thermal remote sensing of surface soil water content with partial vegetation cover for incorporation into climate models. *Journal of Applied Meteorology*, *34*, 745−756.

Gilloes, R. R., Carlson, T. N., Cui, J., Kutas, W. R., & Humes, K. S. (1997). A verification of the 'triangle' method for obtaining surface soil water content and energy fluxes from remote measurements of the Normalized Difference Vegetation Index (NDVI) and surface radiant temperature. *International Journal of Remote Sensing*, *18*(5), 3145−3166.

Granger, R. J. (2000). Satellite-derived estimates of evapotranspiration in the Gediz basin. *Journal of Hydrology*, *229*, 70−76.

Gu, L., Meyers, T., Pallardy, S. G., Hanson, P. J., Yang, B., Heuer, M., et al. (2007). Influences of biomass heat and biochemical energy storages on the land surface fluxes and radiative temperature. *Journal of Geophysical Reasearch*, *107*(D02). doi:10.1029/2006JD007425

Hall, F., Huemmrich, F., Goetz, S. J., Sellers, P. J., & Nikeson, J. E. (1992). Satellite remote sensing of surface energy balance: Success, failures, and unresolved issues in FIFE. *Journal of Geophysical Research*, *97*, 19061−19089.

Harley, P. C., & Tenhunen, J. D. (1991). Modelling the photosynthetic response of C3 leaves to environmental factors. In K. J. Boote & R.S. Loomis (Eds.), *Modelling crop photosynthesis-from biochemistry to canopy* (pp. 17−39). Madison, WI, USA: American Society of Agronomy and Crop Science Society of America.

Haykin, S. (1998). *Neural networks: A comprehensive foundation*, 2nd ed. Englewood Cliffs, NJ: Prentice Hall.

Hogg, E. H. (1994). Climate and the southern limit of the western Canadian boreal forest. *Canadian Journal of Forest Research*, *24*, 1835−1845.

Holdridge, L. R. (1947). Determination of world plant formations from simple climatic data. *Science*, *105*, 367−368.

Hollinger, D. Y., Goltz, S. M., Davidson, E. A., Lee, J. T., Tu, K., & Valentine, H. T. (1999). Seasonal patterns and environmental control of carbon dioxide and water vapor exchange in an ecotonal boreal forest. *Global Change Biology*, *5*, 891−902.

Hollinger, D. Y., Aber, J., Dail, B., Davidson, E. A., Goltz, S. M., Hughes, H., et al. (2004). Spatial and temporal variability in forest-atmosphere CO2 exchange. *Global Change Biology*, *10*, 1689−1706.

Hollinger, S. E., Bernacchi, C. J., & Meyers, T. P. (2005). Carbon budget of mature no-till ecosystem in North Central Region of the United States. *Agricultural and Forest Meteorology*, *130*, 59−69.

Huete, A., Justice, C., & Liu, H. (1994). Development of vegetation and soil indices for MODIS-EOS. *Remote Sensing of Environment*, *49*(3), 224−234.

Hunt, E. R., Piper, S. C., Nemani, R., Keeling, C. D., Otto, R. D., & Running, S. W. (1996). Global net carbon exchange and intra-annual atmospheric CO_2 concentrations predicted by an ecosystem process model. *Global Biogeochemical Cycles*, *10*, 431−456.

Idso, S. B., & Jackson, R. D. (1969). Thermal radiation from the atmosphere. *Journal of Geophysical Research*, *74*, 5397−5403.

Irvine, J., Law, B. E., & Hibbard, K. A. (2007). Postfire carbon pools and fluxes in semiarid ponderosa pine in Central Oregon. *Global Change Biology*, *13*, 1748−1760.

Jackson, T. J., Chen, D., Cosh, M., Li, F., Anderson, M., Walthall, C., et al. (2004). Vegetation water content mapping using Landsat data derived normalized difference water index for corn and soybeans. *Remote Sensing of Environment*, *92*, 475−482.

Jarvis, P. G. (1995). Scaling processes and problems. *Plant, Cell and Environment*, *18*, 1079−1089.

Jenkins, J. P., Richardson, A. D., Braswell, B. H., Ollinger, S. V., Hollinger, D. Y., & Smith, M. -L. (2007). Refining light-use efficiency calculations for a deciduous forest canopy using simultaneous tower-based carbon flux and radiometric measurements. *Agricultural and Forest Meteorology*, *143*, 64−79.

Jiang, L., & Islam, S. (2001). Estimation of surface evaporation map over southern Great Plains using remote sensing data. *Water Resources Research*, *37*(2), 329−340.

Jin, M. L., & Liang, S. L. (2006). An improved land surface emissivity parameter for land surface models using global remote sensing observations. *Journal of Climate*, *19*, 2867−2881.

Jin, Y., Schaaf, C. B., Gao, F., Li, X., Strahler, A. H., Lucht, W., et al. (2003). Consistency of MODIS surface bidirectional reflectance distribution function and albedo retrievals: 1. Algorithm performance. *Journal of Geophysical Research*, *108*(D5). doi:10.1029/2002JD002803

Jin, Y., Schaaf, C. B., Woodcock, C. E., Gao, F., Li, X., Strahler, A. H., et al. (2003). Consistency of MODIS surface bidirectional reflectance distribution function and albedo retrievals: 2. Validation. *Journal of Geophysical Research*, *108*(D5). doi:10.1029/2002JD002804

Justice, C. O., Townshend, J. R. G., Vermote, E. F., Masuoka, E., Wolfe, R. E., Saleous, N., et al. (2002). An overview of MODIS Land data processing and product status. *Remote Sensing of Environment*, *83*, 3−15.

Kalma, J. D., & Jupp, D. L. B. (1990). Estimating evaporation from pasture using infrared thermometry: Evaluation of a one-layer resistance model. *Agricultural and Forest Meteorology*, *51*, 223−246.

Kang, S., Running, S. W., Lim, J., Zhao, M., Park, C., & Loehman, R. (2003). A regional phenology model for detecting onset of greenness in temperate mixed forests. *Korea: an application of MODIS leaf area index Remote Sensing of Environment*, *86*, 232−242.

Kistler, R., et al. (2001). The NCEP–NCAR 50-year reanalysis: monthly means CD-ROM and documentation. *Bulletin of the American Meteorological Society*, *82*, 247−268.

Kjelgaard, J. F., Heilman, J. L., Heilman, K. J., McInnes, K. J., Owens, M. K., & Kamps, R. H. (2008). Carbon dioxide exchange in a subtropical, mixed C3/C4 grassland on the Edwards Plateau, Texas. *Agricultural and Forest Meteorology*, *148*(6), 953−963.

Kustas, W. P., & Norman, J. M. (1996). Use of remote sensing for evapotranspiration monitoring over land surface. *Hydrological Sciences*, *41*(4), 495−515.

Law, B. E., Sun, O. J., Campbell, J., Tuyl, S. V., & Thornton, P. E. (2003). Changes in carbon storage and fluxes in a chronosequence of ponderosa pine. *Global Change Biology*, *9*, 510−524.

Leuning, R., Zhang, Y. Q., Rajaud, A., Cleugh, H. A., & Tu, K. (2008). A simple surface conductance model to estimate evapotranspiration using the Penman–Monteith equation and remote sensing, Water Resour. *Res.*, *44*. doi:10.1029/2007WR006562

Liang, S. L., Zheng, T., Liu, R. G., Fang, H. L., Tsay, Si-Chee, & Running, S. (2006). Estimation of incident photosynthetically active radiation from Moderate Resolution Imaging Spectrometer data. *Journal of Geophysical Research*, *111*, D15208. doi:10.1029/2005JD006730

Lipson, D. A., Wilson, R. F., & Oechel, W. C. (2005). Effects of elevated atmospheric CO2 on soil microbial biomass, activity, and diversity in a chaparral ecosystem. *Applied and Environmental Microbiology*, *71*, 8573−8580.

Ma, S. Y., Baldocchi, D. D., Xu, L. K., & Hehn, T. (2007). Inter-annual variability in carbon dioxide exchange of an oak/grass savanna and open grassland in California. *Agricultural and Forest Meteorology*, *147*, 157−171.

Medrano, H., Flexas, J., & Galmes, J. (2009). Variability in water use efficiency at the leaf level among Mediterranean plants with different growth forms. *Plant and Soil*, *317*, 17−29.

Misson, L., Baldocchi, D. D., Black, T. A., Blanken, P. D., Brunet, Y., Yuste, J. C., et al. (2007). Partitioning forest carbon fluxes with overstory and understory eddy-covariance measurements: A synthesis based on FLUXNET data. *Agricultural and Forest Meteorology*, *144*(1–2), 14−31.

Moffat, A. M., Papale, D., Reichstein, M., Hollinger, D. Y., Richardson, A. D., Barr, A. G., et al. (2007). Comprehensive comparison of gap-filling techniques for eddy covariance net carbon fluxes. *Agricultural and Forest Meteorology*, *147*, 209−232.

Monson, R. K., Turnipseed, A. A., Sparks, J. P., Harley, P. C., Scott-Denton, L. E., Sparks, K., et al. (2002). Carbon sequestration in a high-elevation, subalpine forest. *Global Change Biology*, *8*, 459−478.

Monteith, J. L. (1964). *Evaporation and environment, the state and movement of water in living organismsSymposium of the society of experimental biology, Vol. 19* (pp. 205−234). Cambridge: Cambridge University Press.

Mu, Q. Z., Heinsch, F. A., Zhao, M. S., & Running, S. W. (2007). Development of a global evapotranspiration algorithm based on MODIS and global meteorology data. *Remote Sensing of Environment*, *111*, 519−536.

Myneni, R. B., Hoffman, S., Knyazikhin, Y., Privette, J. L., Glassy, J., Tian Wang, Y., et al. (2002). Global products of vegetation leaf area and fraction absorbed PAR from year one of MODIS data. *Remote Sensing of Environment*, *83*, 214−231.

Osmond, C. B., Winter, K., & Ziegler, Z. (1982). Functional significance of different pathways of CO2 fixation in photosynthesis. In A. Person & H. Zimmerman (Eds.), *Encyclopedia of Plant Physiology, Vol. 12B* (pp. 479−547). New York: Springer-Verlag.

Papale, D., & Valentini, A. (2003). A new assessment of European forests carbon exchange by eddy fluxes and artificial neural network spatialization. *Global Change Biology*, *9*, 525−535.

Penman, H. L. (1948). *Natural Evaporation from Open water, bare soil and grass-Proceedings of the Royal Society of London, A series*, *193*. (pp. 120−145).

Powell, T. L., Gholz, H. L., Clark, K. L., Starr, G., Cropper, W. P., & Martin, T. A. (2008). Carbon exchange of a mature, naturally regenerated pine forest in north Florida. *Global Change Biology*, *14*(11), 2523−2538.

Rammbal, S., Ourcival, J. -M., Offre, R. J., Mouillot, F., Nouvellon, Y., Reichestein, M., et al. (2003). Drought controls over conductance and assimilation of a Mediterranean evergreen ecosystem: Scaling from leaf to canopy. *Global Change Biology*, *9*, 1813−1824. doi:10.1046/j.1529-8817.2003.00687.x

Reichstein, M., Tenhunen, J. D., Roupsard, O., Ourcival, J. M., Rambal, S., Miglietta, F., et al. (2002). Severe drought effects on ecosystem CO_2 and H_2O fluxes at three Mediterranean evergreen sites: Revision of current hypotheses? *Global Change Biology*, *8*, 999−1017. doi:10.1046/j.1365-2486.2002.00530.x

Reichstein, M., Tenhunen, J., Roupsard, O., Ourcival, J. -M., Rambal, S., Miglietta, F., et al. (2003). Inverse modeling of seasonal drought effects on canopy CO2/H2O exchange in three Mediterranean ecosystems. *Journal of Geophysical Reasearch*, *108*(D23), 4726. doi:10.1029/2003JD003430

Reichstein, M., Falge, E., Baldocchi, D., Papale, D., Aubinet, M., Berbigier, P., et al. (2005). On the separation of net ecosystem exchange into assimilation and ecosystem respiration: Review and improved algorithm. *Global Change Biology*, *11*, 1424−1439.

Reichstein, M., Ciais, P., Papale, D., Valentini, R., Running, S., Viovy, N., et al. (2007). Reduction of ecosystem productivity and respiration during the European summer 2003 climate anomaly: A joint flux tower, remote sensing and modelling analysis. *Global Change Biology*, *13*, 634−651. doi:10.1111/j.1365-2486.2006.01224.x

Rumelhart, D. E., Hinton, G. E., & Williams, R. J. (1986). In D. E. Rumelhart & J. L. McClelland (Eds.), *Learning internal representation by error propagationParallel Distributed Processing. Foundations*, *vol. 1*, Cambridge, MA: MIT Press.

Running, S. W., & Coughlan, J. C. (1988). A general model of forest ecosystem processes for regional applications: I. hydrologic balance, canopy gas exchange and primary production processes. *Ecological Modelling*, *42*, 125−154.

Running, S. W., & Hunt, E. R. (1993). Generalization of a forest ecosystem process model for other biomes, BIOME-BGC, and an application for global scale models. In J. Ehleringer & C. Field (Eds.), *Scaling Physiological Process: Leaf to Globe* (pp. 141−158). New York: Academic Press.

Schaaf, C. B., Gao, F., Strahler, A. H., Lucht, W., Li, X., Tsang, T., et al. (2002). First operational BRDF, albedo nadir reflectance products from MODIS. *Remote Sensing of Environment*, *83*, 135−148.

Schapendonk, A. H. C. M., Dijkstra, P., Groenwold, J., Pot, C. S., & Van De Geijn, S. C. (1997). Carbon balance and water use efficiency of frequently cut *Lolium perenne* L swards at elevated carbon dioxide. *Global Change Biology*, *3*, 207−216.

Shuttleworth, W. J., Gurney, R. J., Hsu, A. Y., & Ormsby, J. P. (1989). FIFE: the variation in energy partition at surface flux sites. *Remote Sensing and Large-Scale Global Processes. IAHS Publication*, *186*, 67−74.

Sims, P. L., & Bradford, J. A. (2001). Carbon dioxide fluxes in a southern plains prairie. *Agricultural and Forest Meteorology*, *109*(2), 117−134.

Sims, D. A., Rahmon, A. F., Cordova, V. D., El-Masri, B. Z., Baldocchi, D. D., Bolstad, P. V., et al. (2008). A new model of gross primary productivity for North America ecosystems based solely on the enhanced vegetation index and land surface temperature from MODIS. *Remote Sensing of Environment*, *112*(4), 1633−1646.

Su, Z. (2002). The surface energy balance system (SEBS) for estimation of turbulent heat fluxes. *Hydrology and Earth System Sciences*, *6*, 85−99.

Sugita, M., & Brutsaert, W. (1991). Daily evaporation over a region from lower boundary-layer profiles measured with radiosondes. *Water Resources Research*, *27*(5), 747−752.

Tenhunen, J. D., Sala Serra, A., & Harley, P. C. (1990). Factors influencing carbon fixation and water use by Mediterranean sclerophyll shrubs during summer drought. *Oecologia*, *82*, 381−393.

Urbanski, S., Barford, C., Wofsy, S., Kucharik, C., Pyle, E., Budney, J., et al. (2007). Factors controlling CO2 exchange on timescales from hourly to decadal at Harvard Forest. *Journal of Geophysical Reasearch*, *112*(G2) G02020.

Verma, S. B., Dobermann, A., Cassman, K. G., Walters, D. T., Knops, J. M., Arkebauer, T. J., et al. (2005). Annual carbon dioxide exchange in irrigated and rainfed maize-based agroecosystems. *Agricultural and Forest Meteorology*, *131*, 77−96.

Vermote, E. F., & Vermeulen, A. (1999). MODIS algorithm technical background document—atmospheric correction algorithm: spectral reflectances (MOD09). Version 4.0. http://modis.gsfc.nasa.gov/data/atbd/atbd_mod08.pdf

Wan, Z., Zhang, Y., Zhang, Q., & Li, Z. -L. (2002). Validation of the land-surface temperature products retrieved from Terra Moderate Resolution Imaging Spectro-radiometer data. *Remote Sensing of Environment*, *83*, 163−180.

Whitehead, D. (1998). Regulation of stomatal conductance and transpiration in forest Canopies. *Tree Physiology*, *18*, 633−644.

Williams, M., Malhi, Y., Nobre, A. D., Rastetter, E. B., Grace, J., & Pereira, M. G. P. (1998). Seasonal variation in net carbon exchange and evapotranspiration in a Brazilian rain forest: A modeling analysis. *Plant, Cell and Environment*, *21*, 953−968.

Woodward, F. I. (1987). *Climate and plant distribution.* Cambridge, UK: Cambridge University Press.

Xu, L. K., & Baldocchi, D. D. (2004). Seasonal variation in carbon dioxide exchange over a Mediterranean annual grassland in California. *Agricultural and Forest Meteorology*, *123*, 79−96.

Yi, C., Davis, K. J., Bakwin, P. S., Denning, A. S., Zhang, N., Desai, A., et al. (2004). Observed covariance between ecosystem carbon exchange and atmospheric boundary layer dynamics at a site in northern Wisconsin. *Journal of Geophysical Reasearch*, *109*, D8.

Yu, G. R., Song, X., Wang, Q. F., Liu, Y. F., Guan, D. X., Yan, J. H., et al. (2008). Water-use efficiency of forest ecosystems in eastern China and its relations to climatic variables. *New Phytologist*, *177*, 927−937.

Zhang, Y., Chiew, F. H. S., Zhang, L., Leuning, R., & Cleugh, H. A. (2008). Potential use of evapotranspiration estimates from moderate resolution imaging spectrometer (MODIS) data in predicting runoff at ungauged catchments. *Water Resources Research*, *44*. doi:10.1029/2007WR006563

Zhao, M., Heinsch, F. A., Nemani, R. R., & Running, S. W. (2005). Improvements of the MODIS terrestrial gross and net primary production global data set. *Remote Sensing of Environment*, *95*, 164−176.

Zhao, M., Heinsch, F. A., Nemani, R. R., & Running, S. W. (2006). Sensitivity of Moderate Resolution Imaging Spectroradiometer (MODIS) terrestrial primary production to the accuracy of meteorological reanalyses. *Journal of Geophysical Reasearch*, *111*, G01002. doi:10.1029/2004JG000004, 2006

Zhuang, Q., McGuire, A. D., O'Neill, K. P., Harden, J. W., Romanovsky, V. E., & Yarie, J. (2003). Modeling the soil thermal and carbon dynamics of a fire chronosequence in Interior Alaska. *Journal of Geophysical Reasearch*, *108*(D1).